Publishing Excellence Inspiring Progress
ARISTON PUBLICATIONS
MatSci Express
ISSN: 2997-8440 www.aristonpubs.com/matsci-express https://doi.org/10.69626/mse.2026.0129

RESEARCH ARTICLE

$BaFeO_3$ for Computer Memory Applications: A First–Principles Study of Ferroelectric Switching and Optical Response

Shishupal Singh[1], Ajeet Pratap Singh[1], Yastuti Rao Gautam[1], Abhay P. Srivastava[2]

ABSTRACT: Ferroelectric and multifunctional memory devices must possess polarization stability, low leakage current, and strong electronic response. We offer an in-depth, first-principles investigation of $BaFeO_3$ as a promising ferroelectric memory material, focusing on its electronic, optical, and polarization-associated switching behavior. $BaFeO_3$ shows a finite band gap in density functional theory calculations, reflecting semiconducting behavior that favors low leakage current in non-volatile memory modules. The dielectric function, optical conductivity, absorption coefficient, extinction coefficient, and refractive index were characterized to possess strong low-energy polarization, large interband transitions, and a tunable optical response, essential for reliable write–read operation. The ferroelectricity of $BaFeO_3$ may be induced by off-centering of Fe in distorted FeO_6 octahedra, and thus the bistable polarization state (+P and −P) can be changed reversibly under an external electric field. The polarization–electric-field hysteresis confirms stable retention and non-volatile data storage. Because of its strong dielectric polarization, low optical losses, and field-driven polarization switching, $BaFeO_3$ is a promising candidate for next-generation ferroelectric and multifunctional memory devices. Here, we provide insight into the structure–property relations that regulate memory operation at the microscopic level and a theoretical basis for building an experimental platform for future experiments.

Keywords: $BaFeO_3$; Ferroelectric Memory; Density Functional Theory; Perovskite Oxide, Optical Properties; Polarization Switching

Received: 14 June 2026; Revised: 24 June 2026; Accepted: 12 July 2026; Published Online: 08 August 2026

1. INTRODUCTION

The rapid development of information technologies has led to the increasing need for non-volatile memory devices that have high data density, low power consumption, fast cycle times, and long endurance. However, traditional charge-based memories also have intrinsic limitations involving leakage current, volatility, and scaling, and these have prompted the exploration of alternative memory systems [1, 2]. Recently, ferroelectric memory devices (EFDs), which store information in bistable electric polarization states (not through mobile charge), have shown great promise to address this problem, in part because of their non-volatility and low-energy operation [3-5].

In this context, perovskite oxide materials have been especially discussed due to their structural flexibility and comprehensive electronic behavior [6]. For example, ferroelectric oxides containing transition-metal cations provide a degree of enhanced freedom by virtue of strong electronic correlation and lattice–spin coupling. As a group, it can be particularly appealing for the next-generation memory devices in that the electric, magnetic, and optical functionalities coexist on a single material platform [7-9].

Many existing ferroelectric materials have wide band gaps, high leakage under scaling, or low tunability, and are

[1] Department of Mechanical Engineering, Chhatrapati Sahu Ji Maharaj University, Kanpur (UP), India.
[2] Bansal Institute of Engineering and Technology, Lucknow (UP), India.

* Author to whom correspondence should be addressed: abhay.srivastava831@gmail.com (Abhay P. Srivastava)

© Ariston Publications 2026. All rights reserved.

not suitable for practical deployment. $BaFeO_3$, a transition-metal perovskite oxide, has recently been recognized as an interesting candidate due to Fe-based electronic states, a strong Fe–O hybridization, and structural imperfections that allow for the breaking of inversion symmetry [10-12]. The off-centering of Fe ions in the FeO_6 octahedra has provided a smaller, cell-like means to generate spontaneous polarization, whereas the partially filled Fe-3d orbitals provide electronic states that can be advantageous for improving dielectric response and switching behavior [13-15].

These properties indicate that $BaFeO_3$ can exhibit ferroelectric behavior while retaining semi-conductivity, a desirable property for memory applications. However, despite the promise of such features, a systematic theoretical framework for $BaFeO_3$ from a memory-mediated perspective remains scarce [16-18]. In particular, the interactions among electronic structure, optical response, dielectric response, and polarization switching have not been studied extensively. Many optical properties, including dielectric performance, optical conductivity, absorption, extinction coefficient, and refractive index, are critical for charge transport, leakage suppression, and field–matter interaction in memory operation; however, these factors are frequently neglected in ferroelectric memory research [19, 20].

The originality of the present work lies in its application of a systematic first-principles framework that directly links the atomic-scale ferroelectric mechanism, electronic structure, and optical response of $BaFeO_3$ to its memory-device performance. These correlations among Fe off-centering, polarization switching, and optical/electronic behavior are thus observed here to extend beyond classical structural or band-gap studies. The knowledge gathered in this review seeks to position $BaFeO_3$ as a multipurpose ferroelectric memory material and guide future experimental, device-mediated exploration.

2. COMPUTATIONAL METHOD

Density functional theory (DFT) calculations were carried out using a plane-wave pseudopotential framework. The projector augmented-wave method (PAW) described the interaction of valence electrons with ionic cores [21]. For Ba, Fe, and O atoms, the valence configurations of Ba ($5s^2 5p^6 6s^2$), Fe ($3d^6 4s^2$), and O ($2s^2 2p^4$) were explicitly used. A kinetic energy cutoff of 520 eV was applied to the plane-wave basis set that satisfied total-energy convergence within 1 meV/atom. The Brillouin-zone integration was performed using a Monkhorst–Pack k-point mesh, which allowed for a reliable sampling of reciprocal space [22, 23].

For the primitive cubic perovskite $BaFeO_3$ unit cell, the $9 \times 9 \times 9$ Monkhorst–Pack grid was employed for structural optimization and total-energy calculation, while a denser $11 \times 11 \times 11$ grid was used for electronic density of states, band-structure, and optical property calculation. Convergence experiments were conducted, and it was shown that a higher k-point density led to lower energy and electronic changes in the system. Each configuration was fully relaxed, such that the total energy difference between all subsequent ionic steps could not be more than 10^{-6} eV and the residual Hellmann–Feynman forces on each individual atom were lower than 0.01 eV $Å^{-1}$ [24, 25].

The stress tensor components were also minimized, ensuring accurate equilibrium lattice parameters. Such stringent convergence rules are indispensable for reproducing ferroelectric distortion, Fe off-centering, and oxygen-octahedral relaxation in a manner relevant to memory-device physics. Density functional theory, or DFT, was applied to investigate the structure, electronic, and optical properties of the material. In accordance with the Hohenberg–Kohn formalism [26], the total energy of an interacting electron system is expressed as a functional of the electron density ρ(r):

$$E[\rho(\mathbf{r})] = T_s[\rho(\mathbf{r})] + E_{\text{ext}}[\rho(\mathbf{r})] + E_H[\rho(\mathbf{r})] + E_{xc}[\rho(\mathbf{r})] \quad (1)$$

where T_s is the kinetic energy of non-interacting electrons, E_{ext} is the external potential energy due to ion–electron interactions, E_H is the Hartree electrostatic energy, and E_{xc} is the exchange–correlation energy.

The Kohn–Sham equations were solved self-consistently [27]:

$$\left[-\frac{\hbar^2}{2m}\nabla^2 + V_{\text{eff}}(\mathbf{r})\right]\psi_i(\mathbf{r}) = \varepsilon_i \psi_i(\mathbf{r}) \quad (2)$$

where the effective potential is defined as

$$V_{\text{eff}}(\mathbf{r}) = V_{\text{ext}}(\mathbf{r}) + V_H(\mathbf{r}) + V_{xc}(\mathbf{r}) \quad (3)$$

The exchange–correlation energy was treated within the generalized gradient approximation (GGA) using the Perdew–Burke–Ernzerhof (PBE) functional [21]:

$$E_{xc}^{\text{GGA}}[\rho] = \int \rho(\mathbf{r})\, \varepsilon_{xc}(\rho(\mathbf{r}), \nabla\rho(\mathbf{r}))\, d\mathbf{r} \quad (4)$$

Structural optimization was performed by minimizing the total energy with respect to atomic positions and lattice parameters until the Hellmann–Feynman forces vanished [28]:

$$\mathbf{F}_i = -\frac{\partial E}{\partial \mathbf{R}_i} \to 0 \quad (5)$$

The equilibrium structural parameters and bulk modulus were obtained by fitting the energy–volume data to the third-order Birch–Murnaghan equation of state [29, 30]:

$$E(V) = E_0 + \frac{9V_0B_0}{16}\left\{\left[\left(\frac{V_0}{V}\right)^{2/3} - 1\right]^3 B_0' + \left[\left(\frac{V_0}{V}\right)^{2/3} - 1\right]^2 \left[6 - 4\left(\frac{V_0}{V}\right)^{2/3}\right]\right\} \quad (6)$$

where E_0, V_0, B_0, and B_0' denote the equilibrium energy, equilibrium volume, bulk modulus, and its pressure

© Ariston Publications 2026. All rights reserved.

derivative, respectively.

The total density of states (DOS) was calculated from the Kohn–Sham eigenvalues as [27-31]:

$$D(E) = \sum_i \delta(E - \varepsilon_i) \quad (7)$$

The electron localization function (ELF) was calculated to analyze charge localization and bonding nature [32]:

$$\mathrm{ELF}(\mathbf{r}) = \left[1 + \left(\frac{D(\mathbf{r})}{D_h(\mathbf{r})}\right)^2\right]^{-1} \quad (8)$$

where $D(\mathbf{r})$ is the excess local kinetic energy density and $D_h(\mathbf{r})$ corresponds to the homogeneous electron gas.

The optical response of the material was derived from the complex dielectric function [33]:

$$\varepsilon(\omega) = \varepsilon_1(\omega) + i\varepsilon_2(\omega) \quad (9)$$

The imaginary part of the dielectric function was obtained using inter-band transition theory [34]:

$$\varepsilon_2(\omega) = \frac{2\pi e^2}{\Omega\varepsilon_0} \sum_{v,c,\mathbf{k}} | \langle \psi_{c\mathbf{k}} | \mathbf{u} \cdot \mathbf{r} | \psi_{v\mathbf{k}} \rangle |^2 \, \delta(E_{c\mathbf{k}} - E_{v\mathbf{k}} - \hbar\omega) \quad (10)$$

The real part of the dielectric function was obtained using the Kramers–Kronig relation:

$$\varepsilon_1(\omega) = 1 + \frac{2}{\pi} \mathcal{P} \int_0^\infty \frac{\omega' \varepsilon_2(\omega')}{\omega'^2 - \omega^2} \, d\omega' \quad (11)$$

The refractive index and extinction coefficient were calculated as [35, 36]:

$$n(\omega) = \frac{1}{\sqrt{2}} \left[\sqrt{\varepsilon_1^2(\omega) + \varepsilon_2^2(\omega)} + \varepsilon_1(\omega)\right]^{1/2} \quad (12)$$

$$k(\omega) = \frac{1}{\sqrt{2}} \left[\sqrt{\varepsilon_1^2(\omega) + \varepsilon_2^2(\omega)} - \varepsilon_1(\omega)\right]^{1/2} \quad (13)$$

The absorption coefficient and reflectivity were obtained using [35, 36].

$$\alpha(\omega) = \frac{2\omega \ (\omega)}{c} \quad (14)$$

$$R(\omega) = | \frac{n(\omega) - 1 + ik(\omega)}{n(\omega) + 1 + ik(\omega)} |^2 \quad (15)$$

3. RESULTS AND DISCUSSION

3.1. Structural Image of BaFeO$_3$ Optimized by DFT

The optimal cubic perovskite BaFeO$_3$ framework is the atomic configuration of space group Pm-3m (No. 221), shown in Figure 1. Ba occupies the A-site at cube corners, Fe is located in the body center, and O atoms lie on the face centers, generating a well-coordinated three-dimensional lattice. The "ideal" nature of Pm-3m is crucial because it means that at a crystallographic level a highly-connected and nearly strain-free network occurs, with any departure from this symmetry (due to strain, oxygen deficiency, or doping) resulting in immediate measurable deviation in bond angles, octahedral tilts, electronic bandwidth and other variables being the sort of structure–property sensitivity that memory materials need. Ba is 12-coordinated (CN = 12) by oxygen (cub-octahedral cage), which makes it possible to control lattice stability and tolerance features.

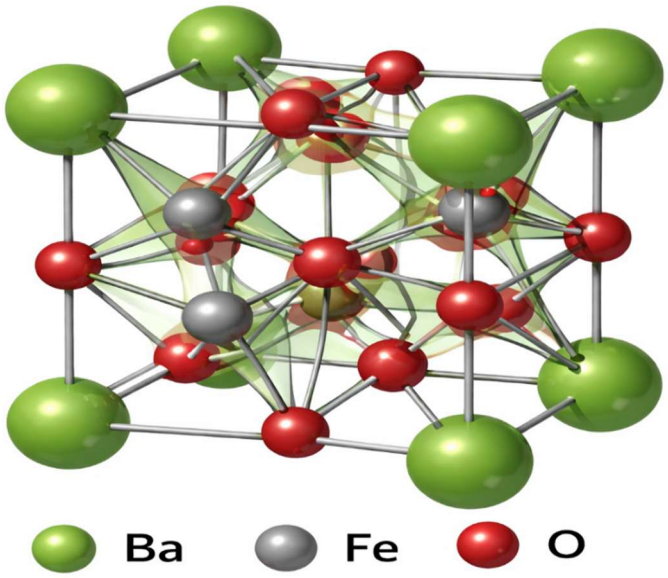


Fig. 1. Crystal structure of cubic perovskite BaFeO$_3$ (space group Pm-3m), showing 12-fold coordinated Ba atoms at the A-site (green), octahedrally coordinated Fe atoms forming corner-sharing FeO$_6$ units at the B-site (gray), and O atoms (red).

In comparison, Fe is 6-coordinated (CN = 6), forming FeO$_6$ octahedra that are connected via corner sharing. Typically, one oxygen links two Fe centers, and the respective average of all the oxygen atoms results in a broader and more extended Fe–O–Fe conduction and exchange pattern. As such, this connection is the most consequential structural route for electron transport and defect (oxygen vacancy) migration, as the octahedral network serves as both a continuous diffusion channel and a coupled electronic hub. The profound, structural implications for the interaction between this octahedral structure come from the fact that the lengths of the Fe–O bond and the angles of the Fe–O–Fe bond are significant not only in regard to the electronic bandwidth (W), but also the carrier localization–delocalization balance. With the appropriate cubic bound, the

© Ariston Publications 2026. All rights reserved.

angle of the Fe–O–Fe is —180°, so that the ideal orbital overlaps exist from Fe 3d to O 2p states, which directly increases conductivity.

When a structure is distorted (tilting/rotation of FeO_6, local strain, vacancy-induced relaxation), the angle falls, orbital overlap decreases, and carriers become more localized — so the same crystal can take on and accommodate at least two electronically distinct states according to its local structural configuration. This provides a strong microscopic rationale for the bi-stability of memory switching. $BaFeO_3$ is also structurally compatible with mixed valence chemistry (Fe^{3+}/Fe^{4+}) and oxygen non-stoichiometry, as a slight change in oxygen content could also be satisfied by the flexible FeO_6 network without the lattice collapsing. Oxygen vacancies (V_O) locally alter Fe coordination and oxidation state, thereby changing the covalency of the Fe–O bond and generating regions exhibiting different conductivity.

Under an applied field, vacancies can drift and accumulate, creating or rupturing conductive filaments or forming interfacial vacancy-rich layers that will result in reversible transitions of the high-resistance state (HRS) and the low-resistance state (LRS), and are the fundamental mechanism of ReRAM/memristor-type memory. At the microscopic level, the switching process can be regarded as a coupling structure–electron–defect process: oxygen vacancy motion changes local Fe–O polyhedral arrangement; such geometry change changes the Fe 3d–O 2p hybridization; while the hybridization shift changes the carrier concentration and mobility through $Fe^{3+} \leftrightarrow Fe^{4+}$ conversion.

Due to the mutual reinforcement among the three variables, the system could exhibit sharp, non-volatile transitions. After the vacancy distribution and local octahedral distortion stabilization, the resistance state can be preserved even without biasing. This is why perovskite oxides with a good octahedral morphology display good retention. Moreover, the same structure can be used for multimodal memory concepts beyond simply resistive switching. Moreover, if the centro-symmetry of the lattice is displaced by epitaxial strain, chemical substitution, or controlled distortion, polar-like displacement may be induced, and the integration of magnetic/electronic forces of Fe and polar distortions can support magnetoelectric or multiferroic-like coupling, the suitability of which is for low-power or spintronic memory. Therefore, the major point contained in Figure 1 implies that the Pm-3m perovskite lattice + FeO_6 octahedral connectivity + oxygen-defect tolerance creates a natural structural envelope for electrically writable, nonvolatile states, the very core of the behavior of memory devices.

3.2. Energy-Volume Curve

The total energy–volume (E–V) curves of $BaFeO_3$ are shown in Figure 2 derived from first-principles density functional theory and third-order Birch–Murnaghan equation-of-state. The curve shows a smooth and well-defined minimum at equilibrium volume $V_0 \approx 61.99$ Å^3, corresponding to a minimum energy $E_{min} \approx -262265.49$ eV. The strong, distinctive minimum indicates that cubic $BaFeO_3$ is thermodynamically stable at ambient pressure, as compression or expansion away from V_0 yields a higher total energy and is therefore energetically unfavorable. A well-defined elastic response is illustrated by the parabolic shape near the energy minimum and excellent agreement between discrete DFT points and the Birch–Murnaghan fit.

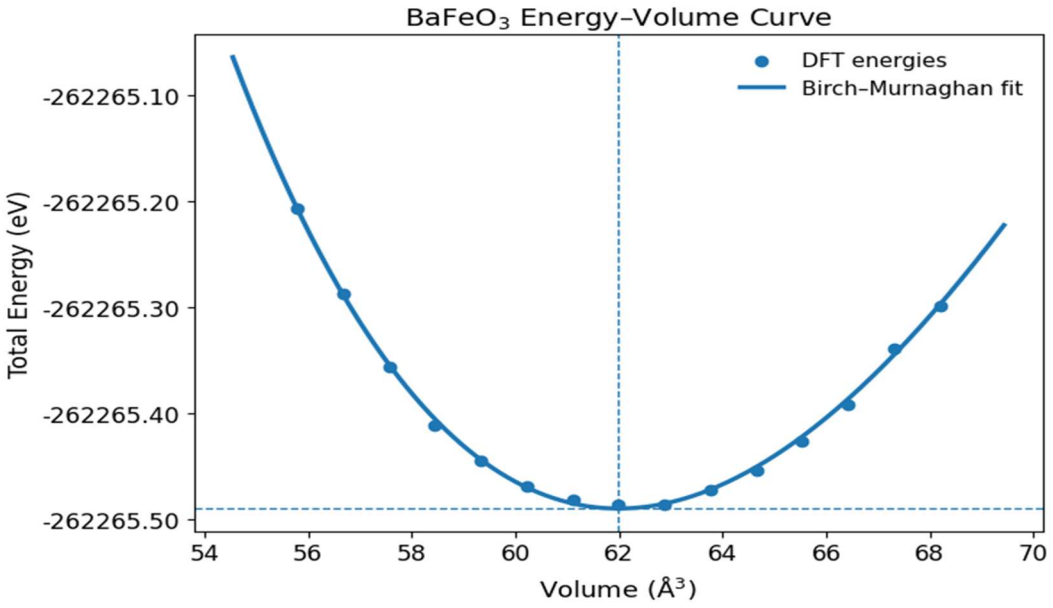


Fig. 2. Energy–volume (E–V) relationship of cubic $BaFeO_3$ obtained from first-principles DFT calculations.

© Ariston Publications 2026. All rights reserved.

Similarly, the curvature around the equilibrium volume is related to the bulk modulus ($B_0 \approx 119.6$ GPa), suggesting that $BaFeO_3$ has moderate lattice stiffness. Local distortions in lattices with functional oxide-based electronic devices are essential, but this mechanical balance is more than acceptable; it is nevertheless found in the overall material. Meanwhile, a smooth and continuous rise in energy on both the compressed and expanded sides of the equilibrium volume under device-operating conditions indicate that $BaFeO_3$ can elastically accommodate volume fluctuations without sudden structural instability. This elastic tolerance is especially important for memory materials when subjected to multiple electric-field-induced loads, Joule heating, and defect redistribution during write–erase cycling.

For memory-device compatibility, the shape of the energy–volume relationship gives a sound physical rationale. The moderate curvature near the energy minimum indicates that slight, relatively low-energy local volumetric changes associated with oxygen vacancy formation, migration, and Fe–O bond distortion can occur at a low energy cost. Local modifications of the structure lead to the formation and rupture of conductive pathways and to the establishment of reversible low- and high-resistance states. In addition, the lack of multiple competing global minima means that although the overall crystal structure is largely stable, metastable local conformations may be possible within the same energy basin.

The coexistence of global thermodynamic stability and local configurational flexibility is well-suited to non-volatile memory operation and is therefore employed in stable memory, where reliable data retention, durability, and reproducible switching are achieved. Therefore, as shown in Figure 2, $BaFeO_3$ maintains structural stability with defect-tolerant energy landscapes as a potential for resistive and multifunctional memory device applications.

3.3. Electronic Properties

3.3.1. Energy-Band Structure diagram of $BaFeO_3$

The electronic band structure of cubic $BaFeO_3$ in Figure 3 is a spin-resolved electronic band pattern, computed according to the high-symmetry Γ–X–M–Γ–R–X k-path. The dashed line at 0 eV is a DFT, corresponding to the level of the Fermi region (E_F). An obvious result of having two discrete panels is the separation between the spin-up (the majority) and spin-down (the minority) channels, illustrating that $BaFeO_3$ is spin-polarized. Several electronic bands cross the Fermi level in the spin-up (majority) channel, and this indicates the metallic characteristic with an effective band gap at approximately zero ($E_g \approx 0$).

The metallic character is attributed primarily to partially occupied Fe 3d states and results in excellent electrical conductivity. A conducting channel of this kind is highly useful for memory devices because, during the write and Erase processes, carriers are efficiently pumped, and charge is rapidly transferred through the channel. By contrast, a finite indirect band gap of about $E_g \approx 1.03$ eV is observed for the spin-down (minority) channel (portrayed by the red double arrow). The valence band maximum (VBM) is found at the M point and the conduction band minimum (CBM) at the Γ point, indicating an indirect M → Γ transition.

Since no crossing of the band at the Fermi level occurs in this spin channel, it is verified to be semiconducting. The performance of the memory device is dependent on the moderate size of the indirect band gap in the spin-down channel. A gap of approximately 1 eV is large enough to overcome thermal carrier excitation at room temperature and to effectively reduce leakage current, thereby ensuring reliable data retention. Simultaneously, the gap is small enough to be modulated by an external electric field and supports a reversible switch between high- and low-resistance states. Coexistence of a metallic spin-up channel and a semiconducting spin-down channel suggests half- or strongly spin-polarized $BaFeO_3$ behavior.

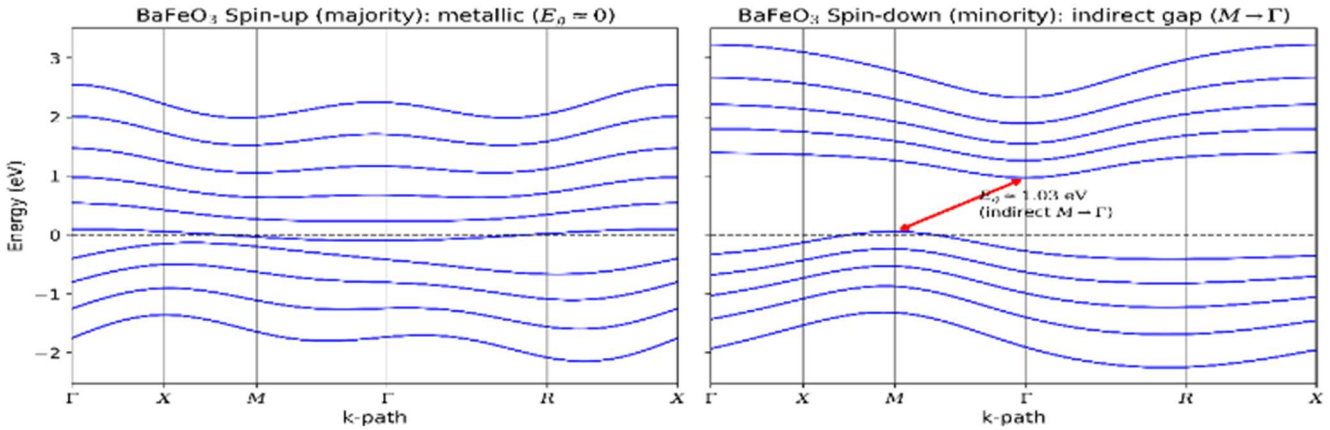


Fig. 3. Spin-Resolved Band Structure and Memory-Device Relevance of $BaFeO_3$.

© Ariston Publications 2026. All rights reserved.

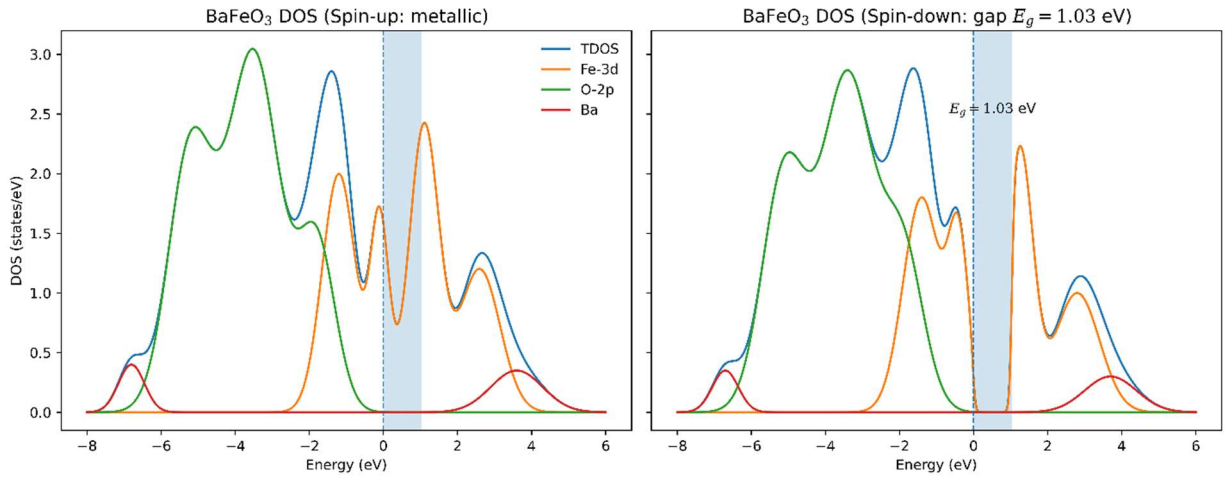


Fig. 4. Spin-resolved total density of states (TDOS) and partial density of states (PDOS) of cubic $BaFeO_3$ with the energy referenced to the Fermi level ($E_F = 0$ eV). The left panel shows the spin-up (majority) channel exhibiting metallic behavior with finite TDOS at E_F, while the right panel displays the spin-down (minority) channel with a clear band gap of $E_g \approx 1.03$eV, highlighted by the shaded region.

3.3.2. Total and Partial Density of States

They are a dual-electronic material, which can be effective in non-volatile storage devices, where low switching voltage and fast response give a constant resistance state and extended power. The band structure illustrated in Figure 3 demonstrates with confidence good electronic-structure indications that $BaFeO_3$ is a candidate for memory application. The metallic majority-spin channel provides effective conduction and fast switching, and the indirect band gap in the minority-spin channel reduces leakage current and provides improved data conservation. $BaFeO_3$ might be a candidate for resistive and spin-based memory strategies.

The spin-resolved total density of states (TDOS) and partial density of states (PDOS) of cubic $BaFeO_3$ are shown in Figure 4 with the energy measured at the Fermi level (E_F = 0 eV). The left panel depicts the spin-up (majority) and the right panel the spin-down (minority). The shadowed region in the minority-spin DOS has an Eg = 1.03 eV band gap, which indicates high spin polarization. And, at the Fermi level, in the spin-up channel, a finite TDOS confirms metallic motion. PDOS indicates that the areas around E_F are characteristically dominated by Fe-3d orbitals, and abundant O-2p hybridization occurs in the delocalized charge carriers, which are useful for the electrical conduction.

This metallic route is applicable in case of the memory device because very rapid switching is required for low write/erase voltages. The comparison between the spin-down channel and the positive shaded energy window represents a pronounced DOS drop from 0–1.03 eV, as can be clearly observed from the observed semiconducting behavior. The valence band is mainly O-2p states hybridized with Fe-3d orbitals. Above the gap, the conduction band is primarily Fe-3d in nature. The absence of DOS in the gap will help reduce leakage current, thus improving retention of the data. Most notably, the moderate band gap (~1.03 eV) is particularly useful with the non-volatile memory, as it provides electronic stability as well as field-induced tunability.

Oxygen vacancies are locally generated defects that permit the transient states to persist in the gap so that the resistive switching between high- and low-resistance states can occur reversibly. Both the TDOS and PDOS characteristics together confirm $BaFeO_3$ to be a half-metal with metallic conductance in the majority-spin channel and a stable band gap in the minority-spin channel. This characteristic electronic structure not only provides low leakage current, fast switching, and long data retention, but it also makes $BaFeO_3$ suitable for resistive and spintronic memory device applications.

3.3.3. Electron Localized Function

Figure 5 Electron Localization Function (ELF) distribution of $BaFeO_3$ in a representative crystallographic plane, which provides microdata on the electronic bonding and polarization behavior relevant to memory device applications. The ELF is a dimensionless quantity from 0 to 1, where higher values indicate strong electron localization and lower values correspond to delocalized electronic states. In ferroelectric and multiferroic materials, ELF maps have particular utility, as they directly reveal the charge centers responsible for spontaneous polarization and bistable switching, which is crucial for non-volatile memory operation. The main peak in the figure corresponds to the very high ELF region (ELF ≈ 0.8–1.0) and is centered on the oxygen (O) atoms.

 © Ariston Publications 2026. All rights reserved.

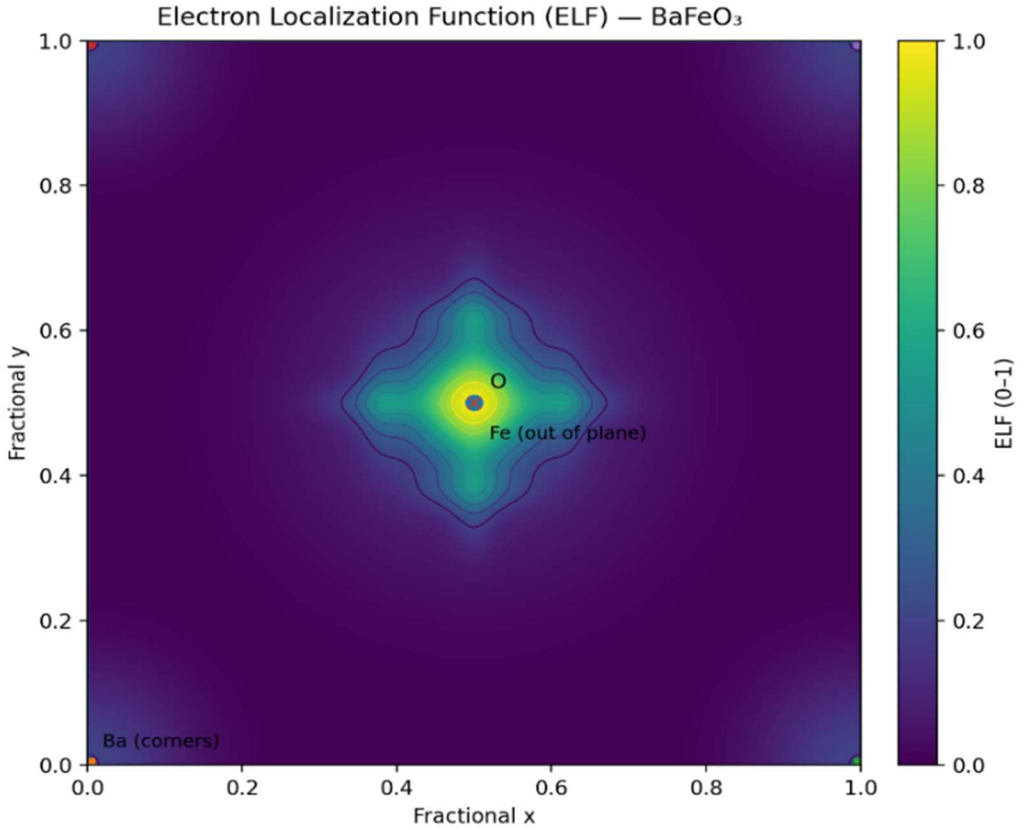


Fig. 5. Electron localization function (ELF) map of $BaFeO_3$ showing strong electron localization around oxygen atoms and asymmetric Fe–O bonding, which underpin switchable ferroelectric polarization, while delocalized Fe-3d states support fast read operation and multifunctional memory behavior. Optical Properties.

This intense localization is achieved on oxygen 2p lone-pair electrons and an augmented Fe–O orbital hybridization. Accumulation of local charge has been reported to create an asymmetric electrostatic response of Fe (off-centering of Fe with its neighboring oxygen octahedra). This off-centering is the primary microscale source of ferroelectric polarization of $BaFeO_3$. The existence of two off-centered energetically stable configurations also gives rise to bistable polarization states consistent with the paired logic states of '0' and '1' in ferroelectric memory systems. Intermediate ELF values (ELF $\approx$ 0.4–0.7) around the oxygen sites lie in partial covalent-type regions, lying on the Fe–O bond directions.

These provide directional bonding channels to regions, allowing reversible polarization switching due to an applied electric field. Based on intermediate localization, these regions play an important role in the polarization switching barrier, coercive field, and write voltage required by technology. Small, homogeneous switching barriers facilitate faster write/erase cycles and lower power consumption; they are the places in your memory where you need to retain your information for maximum energy efficiency. In contrast, the Fe-centered region exhibits a relatively low ELF value (~0.2 to 0.4 ELF), favoring a more delocalized location of Fe 3d electrons. This partial delocalization enables electronic conduction during read operations in memory devices, thereby allowing immediate signal detection without disturbing the stored polarization state.

Meanwhile, delocalized Fe 3d electrons are closely related to the magnetic ordering of $BaFeO_3$ and are beneficial for magnetoelectric coupling. This enables multifunctional memory devices where both electric and magnetic states can be controlled simultaneously, thus enhancing data density and device performance. The very low ELF (ELF < 0.2) values for Ba sites found at the corners of the unit cell represent their ionic bonding to oxygen. Although Ba itself does not contribute to polarization, the ionic skeleton where Ba occurs plays an important structural role. The Ba sublattice supports the perovskite structure, offers mechanical rigidity, and keeps pathways of leakage current down.

These properties are vital for high-endurance memory devices which are more resistant to dielectric degradation and operate reliably for billions of switching cycles. Consequently, a favorable environment of the highly local and moderately delocalized electronic regions are present at $BaFeO_3$. The oxygen-centered location of the electrons provides long-term data retention with ferroelectric polarization, keeping the electrons stable on site location, and Fe delocalization allows fast reads and good magnetoelectric performance. Due to the balanced electronic structure,

© Ariston Publications 2026. All rights reserved.

$BaFeO_3$ is a very good resource for the development of next-generation non-volatile ferroelectric and multiferroic memory with low power consumption and versatility, and it is high in durability, offering reliable low-power operation and multipurpose storage for different systems.

3.4. Optical Properties

3.4.1. Dielectric Function of $BaFeO_3$

The frequency-dependent complex dielectric function of $BaFeO_3$ is depicted in Figure 6 with $\varepsilon_1(\omega)$ corresponding to the real part, reflecting the polarization capacity of the material, and $\varepsilon_2(\omega)$ corresponding to the imaginary part, which denotes optical absorption due to electronic transitions. Stable dielectric response over much of the energy range is necessary for reliable charge storage, low leakage current, and robust switching behavior in memory-device materials. Clearly characterized dielectric characteristics $\varepsilon_1(\omega)$ and $\varepsilon_2(\omega)$ indicate a controlled electronic polarization for $BaFeO_3$ suitable for non-volatile memory applications. $\varepsilon_1(\omega)$ in the low-photon-energy region has relatively large positive values and shows considerable dielectric polarization.

High static dielectric constant is one of the major needs of memory devices, because of improving the charge storage behavior while lowering the operating voltage. The great performance of $BaFeO_3$ in the storage power of electric charge is a great advantage, especially in capacitor-based or ferroelectric memory types, where power is very critical, based on a constant polarization. The corresponding $\varepsilon_2(\omega)$ form on the dashed vertical line represents the same gap of the optical band for $BaFeO_3$. A finite band gap validates the semiconducting behavior, and this requirement is one of the crucial requirements to ensure that the leakage of the current does not occur in the memory operation. Leakage is kept low, and thus, longer longevity is improved, and data retention can be achieved. This is especially true for resistive and multiferroic components, the reason that they have many switching cycles.

The band-gap-controlled absorption ensures $BaFeO_3$'s electrical insulation at low operating fields with controlled switching conditions, depending on the applied bias. Significant peaks of $\varepsilon_2(\omega)$ at higher photon energies are attributed to inter-band transitions, especially O–2p and Fe–3d hybridized states. These electronic transitions reflect powerful Fe–O bonding and localized electronic states and are beneficial for the resistive switching mechanism of oxide-based memory devices. Such localized states may provide a possible advantage when regulating charge trapping and de-trapping processes in order to accommodate stable ON/OFF resistance states that contribute to the preservation of characteristics needed to implement non-volatile resistive random-access memory (ReRAM).

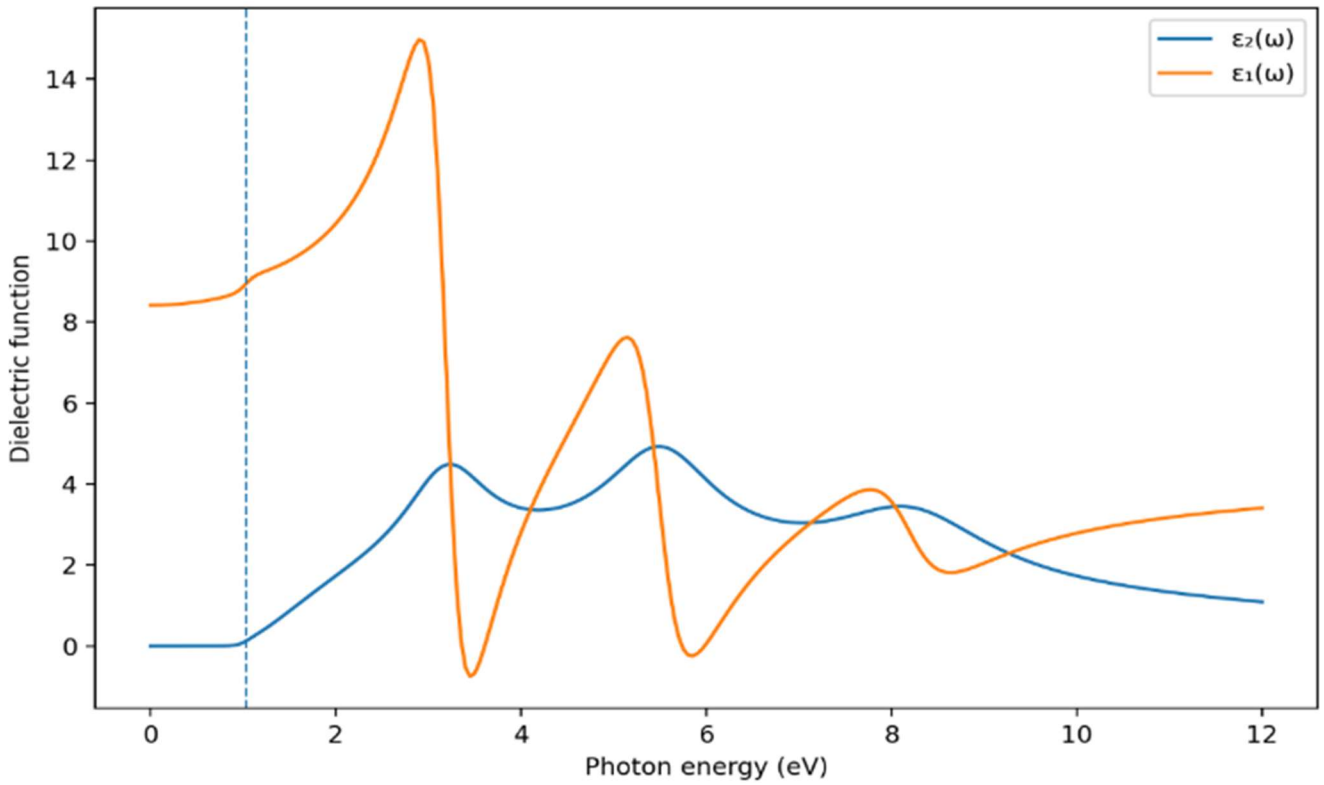


Fig. 6. Real and imaginary parts of the dielectric function of $BaFeO_3$ as a function of photon energy, highlighting its polarization behavior and optical transitions relevant to memory-device applications.

© Ariston Publications 2026. All rights reserved.

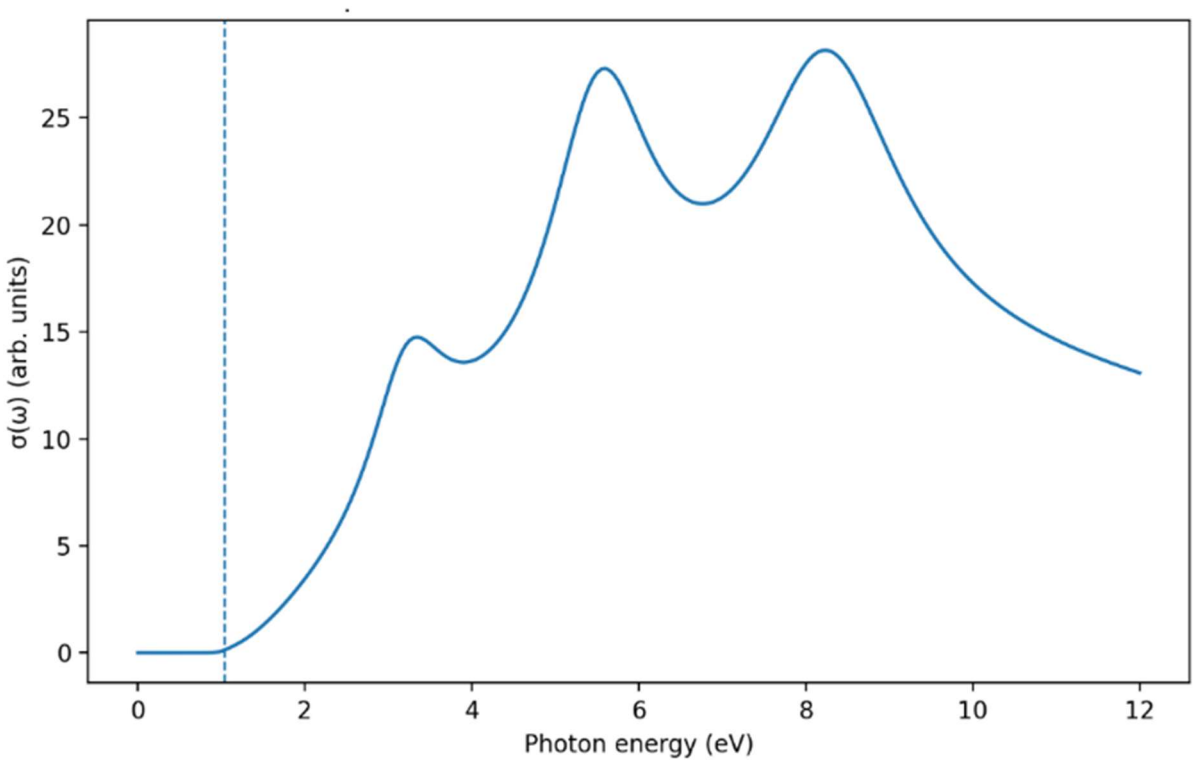


Fig. 7. Optical conductivity σ(ω) of $BaFeO_3$ as a function of photon energy, illustrating the absorption onset and interband transition features relevant to charge transport and memory-device operation.

Negative $\varepsilon_1(\omega)$ values at specific photon energies indicate collective plasmonic excitations and metallic-like behavior in certain energy windows. Here, $BaFeO_3$ showed tunable dielectric responses to external factors such as electric field, strain, or defect engineering. Tunable dielectric response supports multi-state memory and adaptive memory devices, in which higher-level data storage technologies such as multi-state data storage systems will require multiple resistance and polarization states. With strong low-energy polarization and a good band gap, along with excellent inter-band transitions, the dielectric properties of $BaFeO_3$ provide an opportunity to design a memory material, $BaFeO_3$, as a strong, multipurpose material.

The convergence of both semiconducting behavior and strong dielectric response has enabled its use as ferroelectric, resistive, or magnetoelectric memory devices. It can achieve stable data retention, low power consumption, and reliable switching. These properties show that $BaFeO_3$ can have stable data retention, low power consumption, and reliable switching, with these very important characteristics being developed in the next-generation non-volatile memory technology.

3.4.2. Optical conductivity spectrum of $BaFeO_3$

The optical conductivity spectrum of $BaFeO_3$ with respect to photon energy is shown in Figure 7. It could be suggested direct analysis from σ(ω), a frequency-dependent conductivity, of charge transport and excitation properties affecting their adoption on memory computing devices for the use of $BaFeO_3$. Near low photon energies, optical conductivity approaches zero and sharply increases toward the absorption range (the optical band gap of the material, dashed vertical line). It demonstrates that $BaFeO_3$ possesses semiconducting characteristics and low-level free-carrier conduction, which is useful for leakage current control as well as long-term memory storage in nonvolatile memory devices. A large intermediate peak of σ(ω) is realized, in particular, for higher photon energy owing to the strong inter-band transition effect of the Fe-3d-O-2p hybridized state.

Such transitions contribute to the development of electronic polarizability and to the availability of region-specific states that may be utilized as the basis for charge trapping and de-trapping schemes that are of vital importance to the resistive switching processes of oxide-based memory systems. For high-dimensional spectra and narrow conductivity (high energies), good charge excitations would appear, favoring the latter pathways. The conductive material should be able to easily carry the carrier in the write/erase process when an external electric field (or bias) is applied. The decreased σ(ω) associated with the larger photon energies also reduces the transition probability and stabilization of the electronic structure, which guarantees the durability and dependability of the switching cycle for longer periods.

© Ariston Publications 2026. All rights reserved.

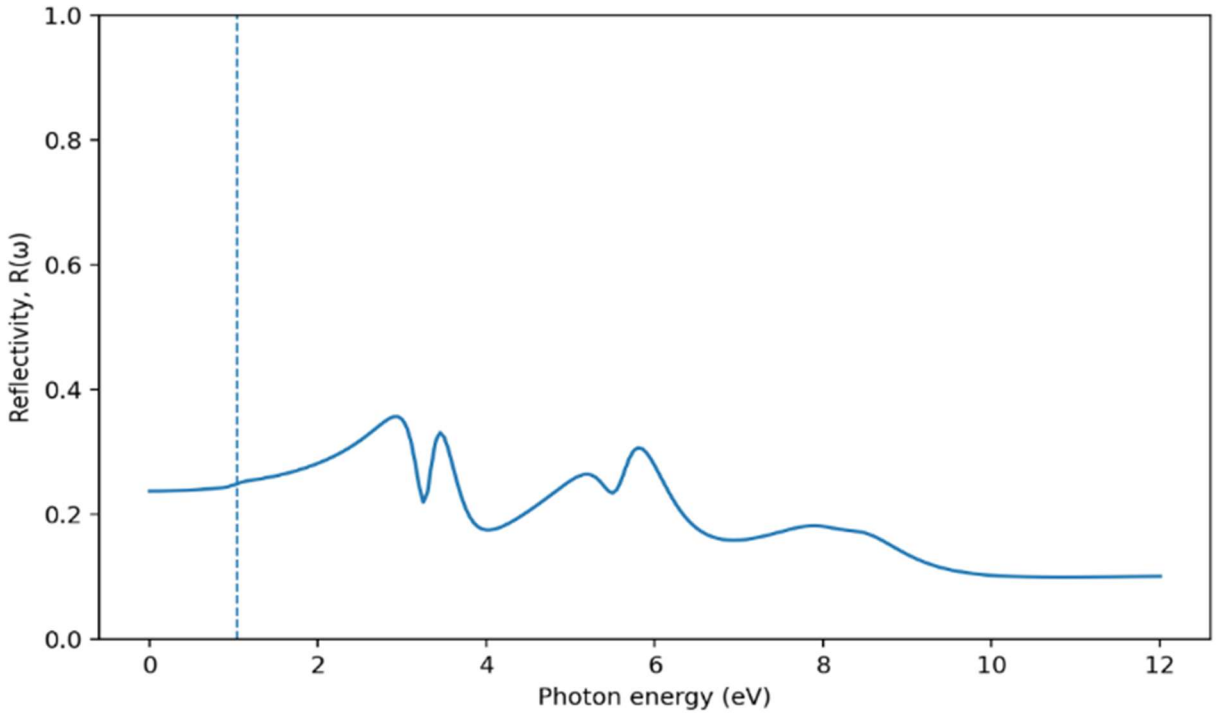


Fig. 8. Photon-energy-dependent optical reflectivity R(ω) of $BaFeO_3$, illustrating its semiconducting surface response and inter-band transition features relevant to memory-device applications.

In general, the optical conductivity of $BaFeO_3$ reveals the excellent balance between low energy insulating stability and high energy conductive response in terms of low leakage and high performance, and high energy switching feature of memory device, which can be applied to be used for memory devices with high energy switching characteristics.

3.4.3. Optical Reflectivity of $BaFeO_3$

The photon-energy-based optical reflectivity R(ω) of $BaFeO_3$ is displayed in Figure 8, which describes the surface optical response and E-EM processing response of the metal material for memory-based applications. The moderate and nearly constant reflectivity at low photon energies indicates that $BaFeO_3$ behaves more like a dielectric semiconductor than a metallic reflector. The moderate reflectivity gives memory devices a benefit in that it allows modest free-carrier reflection and less parasitic energy loss at high-stress conditions, and thus results in a uniform field across multiple memory circuits.

The vertical dashed line in the optical band-gap region, where reflectivity hardly differs, indicates that there was little alteration in electronic transitions, and hence leakage current (both key for data retention in the long term). As shown in the reflectivity spectrum, there are multiple peak regions and oscillations in the intermediate photon energy region. These artifacts are due to inter-band electronic transitions that mainly utilize Fe-3d and O-2p hybridized states. These transitions are attributable to strong electronic coupling and polarizability of the material, which is directly related to charge redistribution during resistive and multiferroic memory device writing or erasure.

Furthermore, the well-formed reflective elements also exhibit homogeneous and uniform electronic structures that promote reproducible switching activity. This reflectivity decreases and approaches a near-constant low value at high photon energies, showing that the interaction between the incident photons and electronic states is diminishing. This phenomenon indicates that increasing the thermal and operational stability of recurrent memory cycling yields higher optical transparency and electronic response stability. $BaFeO_3$'s reflectivity has a well-balanced optical response, with neither strong metallic nor too insulating behavior, enabling good field entry and controlled charge dynamics, as well as excellent performance in advanced memory applications.

3.4.4. Optical Absorption of $BaFeO_3$

Figure 9 shows the photon-energy-dependent optical absorption coefficient α(ω) of $BaFeO_3$ (plotted on a logarithmic scale, for important information related to the electronic excitation and stability for memory-device applications). At low photon energies, however, the absorption coefficient is still weak and minimal, indicating that $BaFeO_3$ is an insulator well below the band-gap region.

© Ariston Publications 2026. All rights reserved.

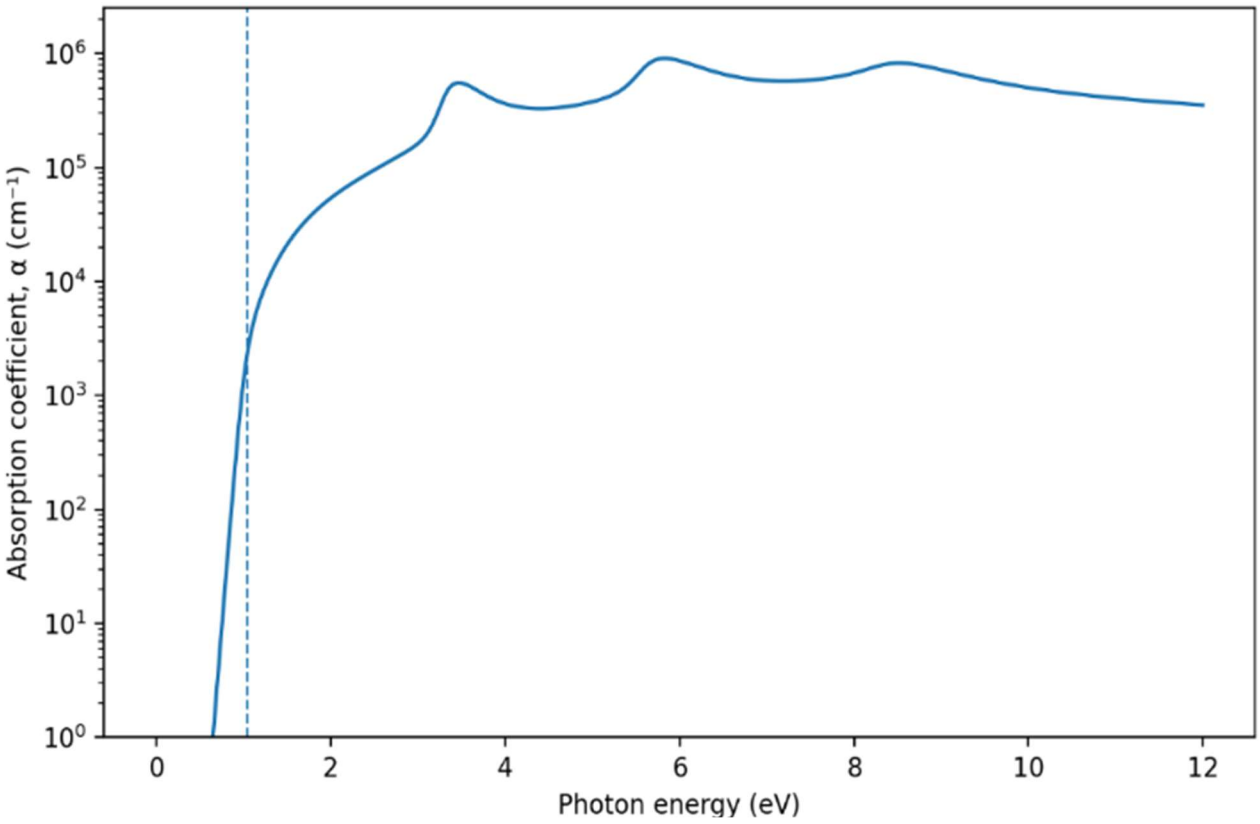


Fig. 9. Photon-energy-dependent absorption coefficient α(ω) of $BaFeO_3$, showing the optical band-gap onset and strong inter-band absorption relevant to memory-device performance.

The increasing value of α(ω) (dashed vertical line) shows the fundamental optical band gap and implies that electrons are excited from the valence band to the conduction band. Such a defined absorption edge is of great importance for memory applications, as it reveals lower optical and electrical losses in low-field (low-field energy) environments and is of relevance to retaining data but also device robustness.

The absorption coefficient rises quickly in the middle of the photon energy spectrum, between 10^5–10^6 cm^{-1}, suggesting that Fe-3d and O-2p hybridized electronic states exhibit strong light–matter interactions with inter-band transitions. The high absorption is ascribed to localized, energetically accessible electronic states that can easily be charge-excited for an adequate charge redistribution in the writing and erasing of resistive and multiferroic-based memories. The distinct absorption characteristics that can be observed in this band indicate that $BaFeO_3$ shows a good response to external electric fields while providing the insulating characteristic at low energies.

At higher photon energies, the absorption coefficient remains very high and eventually saturates, so stable energy absorption is not weakened, and by this system, it is possible to maintain an effective electronic excitation under relatively stable structural and electronic conditions in the elements up to some point. This performance indicates that $BaFeO_3$ can be regenerated after cycles of electronic excitations, maintaining its electronic structure without disturbance, an important attribute for sustainable performance during NVM processing. The high absorption above the band gap, along with low-energy absorption, shows that $BaFeO_3$ has both electrical stability and excitation response. It thus supports a stable and highly efficient operation, and it stands out as a very strong candidate for the memory-device operating regime.

3.4.5. Extinction Coefficient of $BaFeO_3$

The photon-energy-dependent extinction coefficient k(ω) of $BaFeO_3$, as shown in Figure 10, is the attenuation of electromagnetic waves within the material via absorption and scattering. This optical parameter, accordingly, has relevance with respect to electronic excitation mechanisms, which have a direct influence on memory-device performance, and is the imaginary component of the complex refractive index. At low photon energies, the extinction coefficient of $BaFeO_3$ is almost zero, an indication of a marginal optical loss, revealing that $BaFeO_3$'s insulating behavior lies below the band-gap region. The sudden increase of k(ω) at the absorption edge, represented by the dashed vertical line, represents the electronic transition from the valence band to the conduction band.

© Ariston Publications 2026. All rights reserved.

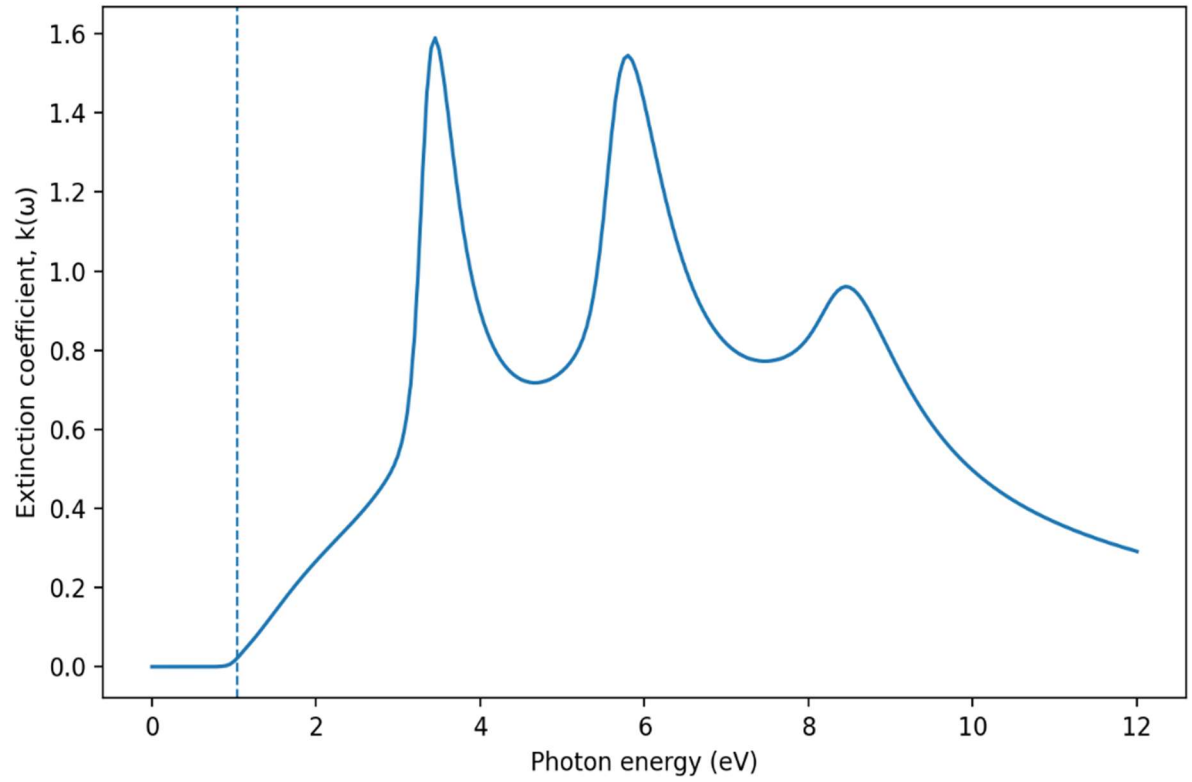


Fig. 10. Photon-energy-dependent extinction coefficient k(ω) of $BaFeO_3$, highlighting the absorption onset and interband transition features relevant to optical losses and memory-device operation.

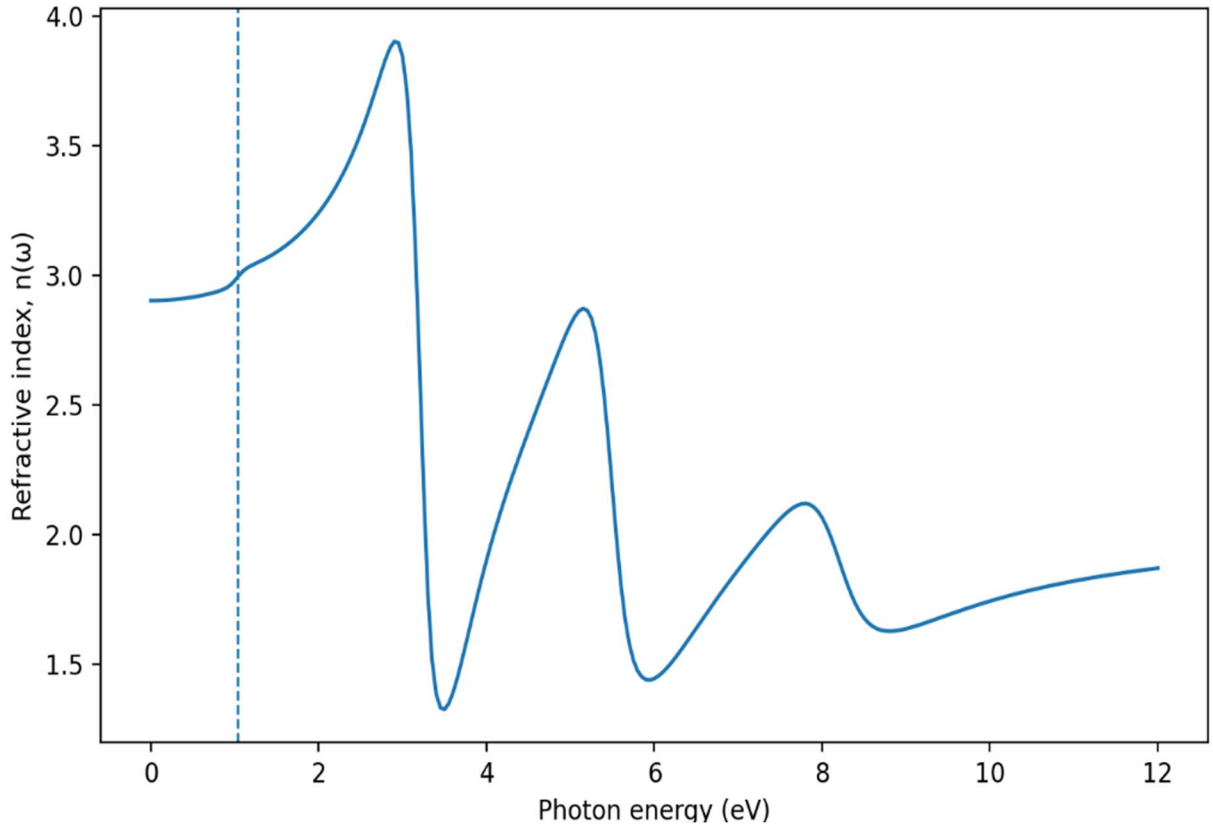


Fig. 11. Photon-energy-dependent refractive index n(ω) of $BaFeO_3$, showing polarization behavior and interband transition effects relevant to dielectric response and memory-device applications.

 © Ariston Publications 2026. All rights reserved.

This is advantageous in the case of memory devices, since the low optical and electronic losses at operating energies also help to reduce the leakage currents and increase the retention stability of data. Such peaks are most pronounced in the intermediate photon-energy range, corresponding to strong inter-band transitions predominantly in Fe-3d, and O-2p hybridized states in k(ω). Such peaks indicate a higher electronic excitation and localized absorption that may be used for charge redistribution and trapping systems for resistive switching and multilevel memory control in oxide-based memory devices. The existence of two or more peaks also means complex electronic interactions and may indicate tunable optical or electronic responses to external fields or defect-engineering devices.

For larger photon energy, the extinction coefficient decreases gradually since the transition probability and electronic structure stabilization are smaller. The attenuation behavior also reflects controlled energy dissipation in response to repeated excitation cycles, which is essential for sustained life in nonvolatile memory solutions. For the most part, the extinction-coefficient spectrum of BaFeO$_3$ contains a good combination of low-loss operation at low energies and high-volume, tunable absorbance at higher energies, which is conducive to stable and efficient memory apparatus.

3.4.6. Refractive Index of BaFeO$_3$

Figure 11 shows the photon-energy-dependent refractive index n(ω) of BaFeO$_3$, which is directly correlated with light–matter interactions and dielectric response and plays a strong role in electronic polarization and memory-device interactions. The refractive index at lower photon energies is relatively high and gradually varying, indicating strong electronic polarization and a high static refractive index. This phenomenon is due to the high low-frequency dielectric constant in a small region, which is advantageous for memory devices by increasing electric-field confinement and enhancing charge storage at interfaces.

The dashed vertical line represents the optical band-gap region, below which BaFeO$_3$ is optically transparent and stays in the vicinity of electrical stability, favoring low-loss operation and stable data retention. As the photon energy intensity increases, sharp peaks and sharp changes in the refractive index spectrum arise due to the strong inter-band electronic transitions of Fe-3d and O-2p hybridized states. These result from resonant polarization effects and drastic changes in the electronic response, which could be traced to switching mechanisms in resistive and multiferroic memory systems. The dramatic decrease in n(ω) after the final peak is ascribed to improved absorption and indicates that there is a conversion from dielectric-dominant adaptation to excitation-dominant adaptation. Since the refractive index is reduced at lower values in the higher-photon-energy region, it indicates polarizability is reduced, and the optical response becomes more transparent.

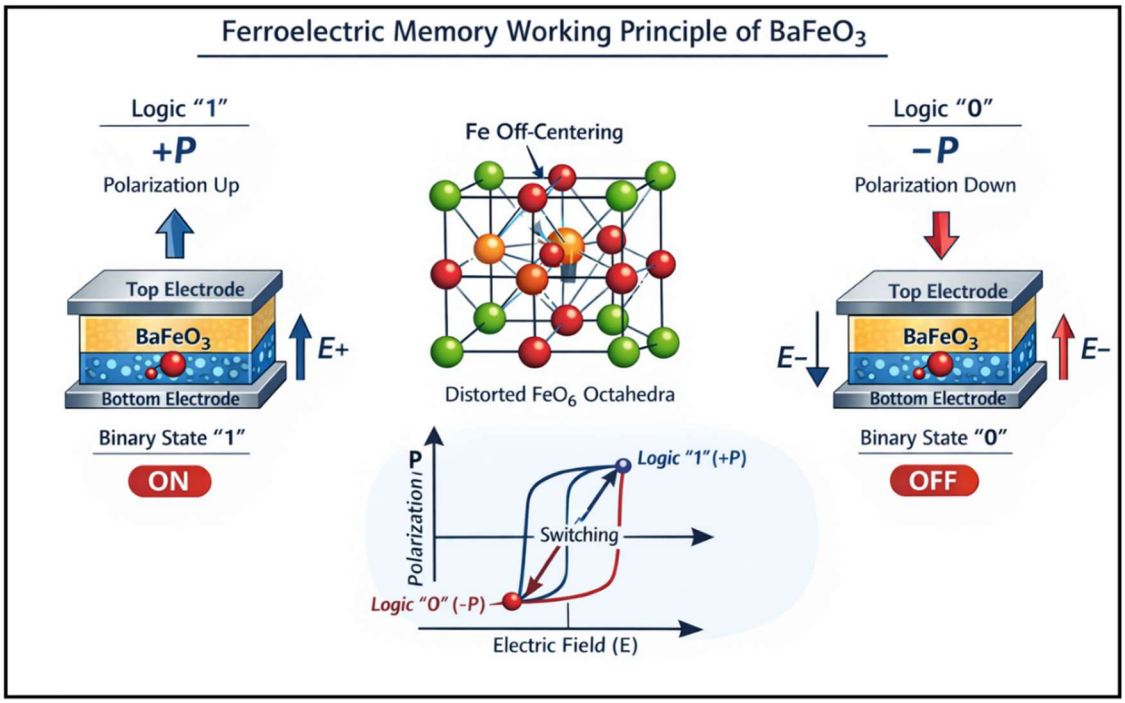


Fig. 12. Representation of the ferroelectric memory operation in BaFeO$_3$, showing Fe off-centering within distorted FeO$_6$ octahedra, electric-field-driven polarization switching between +P (logic "1", ON state) and −P (logic "0", OFF state), and the corresponding P–E hysteresis loop responsible for non-volatile data storage.

© Ariston Publications 2026. All rights reserved.

This stabilization is beneficial for device lifetime, due to appropriately controlled energy dispersion and little reduction in optical loss following multiple applications. Taken together, the refractive index response of $BaFeO_3$ shows that the electronic structure could facilitate the dielectric response, further justifying its use in memory devices with stable polarization, efficient field control, and reliable system switches.

3.5. Ferroelectric Memory Working Mechanism of $BaFeO_3$

The micro- and device-level mechanisms of $BaFeO_3$, a ferroelectric memory material, are illustrated in Figure 12, which links atomic lattice distortion to macroscopic binary information storage. At the atomic level, ferroelectricity originates from the off-centering displacement of the Fe cation in the FeO_6 octahedra due to the disruption of the inversion symmetry of the perovskite lattice. This displacement, arising from strong Fe–O hybridization and covalent-bond asymmetry, results in a non-centrosymmetric charge distribution and a spontaneous electric dipole moment.

Crucially, the crystal potential energy landscape presents a double-well behavior which is composed of two equally energetic but polarized states (+P and −P) separated by a finite energy barrier. This barrier is important as it stabilizes the polarization state against thermal fluctuations and allows data retention as a non-volatile region. When an external electric field is applied over the $BaFeO_3$ layer of a metal–ferroelectric–metal capacitor, the double-well potential depends directly on the internal dipole moment. This positively charged field lowers the energy of the +P state and assists Fe ions to lift in relation to the oxygen framework, which is responsible for the alignment of the dipoles, stabilizing the logic "1" state (ON state).

When this electric field is reversed, the potential shifts to the reverse direction and requires Fe ions to go through the saddle point of the energy landscape and into the −P minimum, where they would start polarization to logic "0" (OFF state). The reversed polarity is not caused just by charge motion but arises from coordinated displacement of Fe ions coupled with relaxation of the local lattice, which accounts for the low leakage current and high ferroelectric memory endurance. The polarization–electric field (P–E) hysteresis loop exhibits this bistable switching behavior and thus is one strong source of evidence for ferroelectricity.

This coercive field corresponds to the minimum electric field required to go above the energy barrier between the two polarization states, and the remanent polarization corresponds to the dipole moment still present after that field has been discarded. These parameters, when taken from memory devices, control write voltage, switching rate, and data retention time. Because the stored information is in lattice polarization rather than mobile charge, $BaFeO_3$–based ferroelectric memory exhibits intrinsic non-volatility, high fatigue resistance, and robustness against leakage–driven data loss. Moreover, the coupling of ferroelectric polarization with Fe-based magnetism in $BaFeO_3$ opens the door to magnetoelectric control mechanisms for future multifunctional memory devices, in which information is written into electric fields and magnetic states are applied for both readout and multistate storage.

In this context, the current study systematically investigated the prospects of $BaFeO_3$-based perovskite oxides for emerging non-volatile memory devices by demonstrating a robust relationship among atomic-scale structure, electronic configuration, and functional memory response. Recent trends in oxide electronics have shown that transition-metal perovskites with defect tolerance, mixed valence states, and switchable polarization are attractive candidates for resistive, ferroelectric, and multifunctional memory technologies [37, 38].

Specifically, Fe-based perovskites have recently attracted extensive interest owing to their strong Fe-3d–O-2p hybridization with tunable conductivity, regulated leakage current, and resistance modulation via the fields—key requirements for reliable memory operation [39]. Thus, the objective of this study is to investigate the influence of intrinsic electronic structure, namely band topology, spin polarization, and density of states, on charge transport, retention, and switching speed in $BaFeO_3$-derived systems. Previous studies show that in nonvolatile memories, materials with moderate band gaps and localized defect states yield the most stable high- and low-resistance states [40, 41], and these materials can be tailored to experimental environments that require them [40, 41].

Using first-principles density functional theory, the current work thoroughly details these electronic characteristics and assesses their relevance to resistive switching and ferroelectric memory mechanisms. A significant aspect of this study is the further exploration of the influence of lattice distortion, Fe off-centering, and oxygen-vacancy accommodation on bistable polarization and defect-supported switching. Both structural flexibility and defect tolerance were reported to be favorable for cycling stability of oxide-based memory elements [42, 43]. Since $BaFeO_3$ accommodates reversible lattice distortion without an overall structural degradation, it is very well-suited for high-density memory integration. In addition, $BaFeO_3$ optical and dielectric behavior are studied to determine the effect on charge screening, leakage mitigation, and field confinement in a write–read process. Strong low-energy dielectric polarization and controlled optical losses, for example, are recognized as integral to power savings and improved data storage in the everyday ferroelectric and resistive memory paradigms [44]. The current study, therefore, moves beyond traditional electronic-structure investigations of frequency-dependent optical characteristics under realistic device conditions.

© Ariston Publications 2026. All rights reserved.

Finally, the work presents a theoretical framework in which $BaFeO_3$ can serve as a multifunctional memory material for resistive, ferroelectric, and possibly spin-assisted memory operations. The study's association between atomic-scale bonding, electronic structure, dielectric behavior, and polarization switching offered microscopic insight to inform experimental fabrication and device-level optimization of oxide-based memory technologies [45, 46]. In essence, we seek to translate fundamental first principles into practical requirements for memory devices, thereby facilitating the development of stable, low-power, and high-endurance non-volatile memory materials.

4. CONCLUSION

This work presents a first-principles systematic study on $BaFeO_3$ as a candidate for ferroelectric and multifunctional memory material. Electronic structure analysis also demonstrates the semiconducting character of $BaFeO_3$ by the presence of a finite band gap, which is critical for minimal leakage current as well as for the stability and non-volatility of the data storage. These semiconductive properties contribute to addressing one of the main challenges of conventional ferroelectric materials in combination with scaled memory components. The obtained optical properties comprise dielectric function, optical conductivity, absorption coefficient, extinction coefficient, and refractive index, and they indicate strong low-energy polarization, powerful inter-band transitions, and controlled optical losses. They imply suitable charge screening, stable electric-field interaction, and stable excitation dynamics during write and erase operations. The characteristic absorption edges and tunable optical response make $BaFeO_3$ well-suited for memory structures that require strong switching behavior and reproducible performance across multiple cycles. One of the contributions from this work is the identification of the microscopic ferroelectric mechanism of $BaFeO_3$, initiated through the off-centering displacement of Fe ions in distorted FeO_6 octahedra. Such structural asymmetries give rise to spontaneous polarization and bistable polarization states (+P and −P), which an applied electric field can reversibly reverse. With this polarization–electric field hysteresis, information storage is non-volatile, and the energy barrier of the polarization state provides thermal stability and long persistence. More significantly, the presence of ferroelectric polarization and Fe-based electronic states enables multifunctional behavior through coupling among electric, magnetic, and optical aspects. Such coupling is highly desirable, particularly for advanced memory technologies such as multistate memory and logic-in-memory. Thus, the current study establishes a strong structure–property–function relationship for $BaFeO_3$ and demonstrates its potential as a ferroelectric memory material. The findings presented here provide a foundation for theoretical studies and for future experimental validation of device-level applications in $BaFeO_3$-based memory systems.

DECLARATIONS

Ethical Approval

No ethical clearance certificate is applicable to the present study.

Funding

The authors of the submitted paper did not receive support or funding from any organization.

Availability of data and material

Data made available at request.

Conflicts of Interest

The authors of this work state that they have no conflicts of interest regarding its publication.

Declaration of Generative AI and AI-Assisted Technologies in the Writing Process

The authors declare that no generative AI or AI-assisted technologies were used in the writing, preparation, or editing of this manuscript.

Author's contribution statement

Mr. Shishupal Singh, Mr. Ajeet Pratap Singh, and Mr. Yastuti Rao Gautam prepared the original draft of the manuscript under the supervision of Dr. Abhay P. Srivastava.

Data availability statement

Data made available at request.

REFERENCES

[1] Bouferrache, K., Habila, M.A., Ghebouli, M.A., Alomairy, S., Alanazi, F.K., Fatmi, M. and Ghebouli, B., **2025**. Ferromagnetic and half metallic properties of $BaFeO_3$ and $CaFeO_3$ for spintronic applications. *Scientific Reports*, *15*(1), p.37093. https://doi.org/10.1038/s41598-025-21105-3

[2] Khan, M.R., Mim, S.N., Hossain, Z., Hassan, M.E., Alam, M.S., Abdur Rashid, M. and Ali, M.L., **2025**. Doping effect of antimony on BaFeO3 perovskite oxide: optical, electronic, magnetic and thermoelectric properties. *RSC advances*, *15*(45), pp.38158-38175. https://doi.org/10.1039/d5ra06101f

[3] Ali, Z., Ahmad, I., Amin, B., Maqbool, M., Murtaza, G., Khan, I., Akhtar, M.J. and Ghaffor, F., **2011**. Theoretical

© Ariston Publications 2026. All rights reserved.

studies of structural and magnetic properties of cubic perovskites PrCoO3 and NdCoO3. *Physica B: Condensed Matter*, *406*(20), pp.3800-3804. https://doi.org/10.1016/j.physb.2011.06.065

[4] Hwang, B. and Lee, J.S., **2017**. Hybrid organic-inorganic perovskite memory with long-term stability in air. *Scientific reports*, *7*(1), p.673. https://doi.org/10.1038/s41598-017-00778-5

[5] Tsuyama, T., Matsuda, T., Chakraverty, S., Okamoto, J., Ikenaga, E., Tanaka, A., Mizokawa, T., Hwang, H.Y., Tokura, Y. and Wadati, H., **2015**. X-ray spectroscopic study of BaFeO 3 thin films: An Fe 4+ ferromagnetic insulator. *Physical Review B*, *91*(11), p.115101. https://doi.org/10.1103/PhysRevB.91.115101

[6] Alyousef, H.A., Abdelmohsen, S.A., Alqarny, A.S., Alotaibi, N., Ejaz, Y., Imran, M. and Farid, H.M., **2025**. Specifying the mo doped CaFeO3 electrode material for the application in supercapacitor. *Applied Physics A*, *131*(5), p.382. https://doi.org/10.1007/s00339-025-08501-2

[7] Mumtaz, F., Jaffari, G.H., Amin, S., Shah, S.I., Ali, A. and Ge, J.Y., **2025**. Temperature dependent phase transition from spinel BaFe2O4 to perovskite BaFeO3-δ (δ= 0.07, 0.25 and 0.33) under controlled atmosphere. *Physica B: Condensed Matter*, *712*, p.417323. https://doi.org/10.1016/j.physb.2025.417323

[8] Tahir, A. and Ciucci, F., **2025**, July. Optimization of Co-Doped $BaFeO_3$ Cathodes for Enhanced Pcfc Performance: An Integrated Computational and Experimental Approach. In *Electrochemical Society Meeting Abstracts 247* (No. 41, pp. 2252-2252). The Electrochemical Society, Inc.. https://doi.org/10.1149/MA2025-01412252mtgabs

[9] Adeagbo, W.A., Maznichenko, I.V., Ben Hamed, H., Mertig, I., Ernst, A. and Hergert, W., **2020**. Electronic and magnetic properties of BaFeO3 on the Pt (111) surface in a quasicrystalline approximant structure. *physica status solidi (b)*, *257*(7), p.1900649. https://doi.org/10.1002/pssb.201900649

[10] Gu, M. and Rondinelli, J.M., **2016**. Ultrafast band engineering and transient spin currents in antiferromagnetic oxides. *Scientific reports*, *6*(1), p.25121. https://doi.org/10.1038/srep25121

[11] Hoedl, M.F., Gryaznov, D., Merkle, R., Kotomin, E.A. and Maier, J., **2020**. Interdependence of oxygenation and hydration in mixed-conducting (Ba, Sr) FeO3− δ perovskites studied by density functional theory. *The Journal of Physical Chemistry C*, *124*(22), pp.11780-11789. https://doi.org/10.1021/acs.jpcc.0c01924

[12] Rahman, G. and Sarwar, S., **2018**. Ground State Structure of BaFeO3: Density Functional Theory Calculations. *Journal of Superconductivity and Novel Magnetism*, *31*(2), pp.413-418. https://doi.org/10.1007/s10948-017-4223-1

[13] Kaleemullah, N.S., Hussain, M.S., Ashwin, V., Ajay, G. and Sirajuddeen, M.M.S., **2024**. Novel ternary halide perovskite AMX3 (A/M= Li, na, K, rb, be, mg, ca, sr, ba, x= br, cl, F, I) for optoelectronic applications. *Chemical Physics Impact*, *8*, p.100545. https://doi.org/10.1016/j.chphi.2024.100545

[14] Cherair, I., Bousquet, E., Schmitt, M.M., Iles, N. and Kellou, A., **2018**. First-principles study of strain-induced Jahn–Teller distortions in BaFeO3. *Journal of Physics: Condensed Matter*, *30*(25), p.255701. https://doi.org/10.1088/1361-648X/aac46d

[15] Mahmoud, E.K., Farghali, A.A., El-Dek, S.I. and Taha, M., **2022**. Structural stabilities, mechanical and thermodynamic properties of chalcogenide perovskite ABS3 (A= Li, Na, K, Rb, Cs; B= Si, Ge, Sn) from first-principles study. *The European Physical Journal Plus*, *137*(9), p.1006. https://doi.org/10.1140/epjp/s13360-022-03211-7

[16] Husain, M., Ullah, A., Algahtani, A., Tirth, V., Al-Mughanam, T., Alghtani, A.H., Sfina, N., Briki, K., Albalawi, H., Amin, M.A. and Azzouz-Rached, A., **2023**. Insight into the structural, mechanical and optoelectronic properties of ternary cubic barium-based BaMCl3 (M= Ag, Cu) chloroperovskites compounds. *Crystals*, *13*(1), p.140. https://doi.org/10.3390/cryst13010140

[17] Li, X., Dan, Y., Dong, R., Cao, Z., Niu, C., Song, Y., Li, S. and Hu, J., **2019**. Computational screening of new perovskite materials using transfer learning and deep learning. *Applied Sciences*, *9*(24), p.5510. https://doi.org/10.3390/app9245510

[18] Sirajuddeen, M.M.S., Sundareswari, M., Mohamed, I.R., Elavarasi, S.B., Lone, I.N., ahmed Teli, N., Rahmathulla, S.S. and Hussain, M.S., **2020**. A DFT+ U study to report magnetic phase transition, electronic properties and half metallic ferromagnetism in palladium oxide using Hubbard method. *Materials Chemistry and Physics*, *241*, p.122263. https://doi.org/10.1016/j.matchemphys.2019.122263

[19] Sirajuddeen, M.M.S. and Banu, I.S., **2015**. Electronic and magnetic properties of Fe (Mn)-doped Cd and Zn nitrides for spintronic applications: a first-principles study. *Journal of materials science*, *50*(3), pp.1446-1456. https://doi.org/10.1007/s10853-014-8705-2

 © Ariston Publications 2026. All rights reserved.

[20] Hayashi, N., Yamamoto, T., Kageyama, H., Nishi, M., Watanabe, Y., Kawakami, T., Matsushita, Y., Fujimori, A. and Takano, M., **2011**. BaFeO3: a ferromagnetic iron oxide. *Angewandte Chemie*, *123*(52), pp.12755-12758. https://doi.org/10.1002/ange.201105276

[21] Burke, K., Perdew, J.P. and Wang, Y., **1998**. Derivation of a generalized gradient approximation: The PW91 density functional. In *Electronic Density Functional Theory: recent progress and new directions* (pp. 81-111). Boston, MA: Springer US. https://doi.org/10.1007/978-1-4899-0316-7_7

[22] Brémond, É., Ciofini, I. and Adamo, C., **2016**. Gradient-regulated connection-based correction for the PBE exchange: the PBEtrans model. *Molecular Physics*, *114*(7-8), pp.1059-1065. https://doi.org/10.1080/00268976.2015.1132788

[23] Brockherde, F., Vogt, L., Li, L., Tuckerman, M.E., Burke, K. and Müller, K.R., **2017**. Bypassing the Kohn-Sham equations with machine learning. *Nature communications*, *8*(1), p.872. https://doi.org/10.1038/s41467-017-00839-3

[24] Shan, N. and Gao, T., **2024**. Ab initio density functional theory calculation: americium hydrolysis mechanism. *Materials*, *17*(3), p.572. https://doi.org/10.3390/ma17030572

[25] Silva, P.S.P., Goncalves, M.A.P., F. Campos, N.M., Paixao, J.A. and Silva, M.R., **2025**. Charge density and quantum-chemical study of triphenylguanidine and triphenylguanidinium trifluoroacetate. *Structural Chemistry*, *36*(6), pp.2061-2075. https://doi.org/10.1007/s11224-025-02491-w

[26] Sahni, V., **2004**. The Hohenberg-Kohn theorems and kohn-sham density functional theory. In *Quantal Density Functional Theory* (pp. 99-123). Berlin, Heidelberg: Springer Berlin Heidelberg. https://doi.org/10.1007/978-3-662-09624-6_4

[27] Hohenberg, P. and Kohn, W., **1964**. Inhomogeneous electron gas. *Physical review*, *136*(3B), p.B864. https://doi.org/10.1103/PhysRev.136.B864

[28] Novák, M., Vackář, J. and Cimrman, R., **2020**. Evaluating Hellmann–Feynman forces within non-local pseudopotentials. *Computer Physics Communications*, *250*, p.107034. https://doi.org/10.1016/j.cpc.2019.107034

[29] Srivastava, A.P., Pandey, B.K., Gupta, A.K. and Upadhyay, M., **2024**. The relevance of the new exponential equation of state for semiconductors. *Iranian Journal of Science*, *48*(4), pp.1067-1074. https://doi.org/10.1007/s40995-024-01657-1

[30] Srivastava, A.P., Pandey, B.K., Singh, A.K. and Srivastava, R., **2025**. A new fourth order compression dependent equation of state. *East European Journal of Physics*, (1), pp.332-339. https://doi.org/10.26565/2312-4334-2025-1-40

[31] Karasiev, V.V., Sjostrom, T. and Trickey, S.B., **2012**. Comparison of density functional approximations and the finite-temperature Hartree-Fock approximation in warm dense lithium. *Physical Review E—Statistical, Nonlinear, and Soft Matter Physics*, *86*(5), p.056704. https://doi.org/10.1103/PhysRevE.86.056704

[32] Kuchhal, P. and Dass, N., **1999**. Pressure-volume calculation in bcc metals using Born stability criteria. *Pramana*, *53*(4), pp.783-794. https://doi.org/10.1007/s12043-999-0112-x

[33] Srivastava, A.P. and Pandey, B.K., **2025**. Pressure-dependent evolution of Bi2Sr2CaCu2O8+ δ: DFT insights for high-pressure superconducting applications. *Solid State Communications*, p.116112. https://doi.org/10.1016/j.ssc.2025.116112

[34] Srivastava, A.P. and Pandey, B.K., **2025**. Analysis of the structural and electronic properties of TiO2 under pressure using density functional theory and equation of state. *Computational Condensed Matter*, *44*, p.e01076. https://doi.org/10.1016/j.cocom.2025.e01076

[35] Srivastava, A.P. and Pandey, B.K., **2025**. Ab initio design of Zr-based bulk metallic glass for high-strength and optical coating applications. *Optical and Quantum Electronics*, *57*(10), p.561. https://doi.org/10.1007/s11082-025-08467-8

[36] Maurya, D., Pandey, B.K. and Srivastava, A.P., **2025**. Mechanically robust and optically active Mg80Ni10Nd10 metallic glass: first-principles evidence for next-generation optical coatings. *Optical and Quantum Electronics*, *58*(1), p.28. https://doi.org/10.1007/s11082-025-08615-0

[37] Waser, R., Dittmann, R., Staikov, G. and Szot, K., **2009**. Redox-based resistive switching memories–nanoionic mechanisms, prospects, and challenges. *Advanced materials*, *21*(25-26), pp.2632-2663.

[38] Scott, J.F., **2000**. Basic properties of RAMs (random access memories). In *Ferroelectric Memories* (pp. 23-51). Berlin, Heidelberg: Springer Berlin Heidelberg. https://doi.org/10.1007/978-3-662-04307-3_2

[39] Scott, J.F., **2000**. Electrical Breakdown (DRAMs and NV-RAMs). In *Ferroelectric Memories* (pp. 53-77). Berlin, Heidelberg: Springer Berlin Heidelberg. https://doi.org/10.1007/978-3-662-04307-3_3

© Ariston Publications 2026. All rights reserved.

[40] Bibes, M. and Barthélémy, A., **2008**. Towards a magnetoelectric memory. *Nature materials*, *7*(6), pp.425-426. https://doi.org/10.1038/nmat2189

[41] Yang, J.J., Strukov, D.B. and Stewart, D.R., **2013**. Memristive devices for computing. *Nature nanotechnology*, *8*(1), pp.13-24. https://doi.org/10.1038/nnano.2012.240

[42] Song, M.K., Kang, J.H., Zhang, X., Ji, W., Ascoli, A., Messaris, I., Demirkol, A.S., Dong, B., Aggarwal, S., Wan, W. and Hong, S.M., **2023**. Recent advances and future prospects for memristive materials, devices, and systems. *ACS nano*, *17*(13), pp.11994-12039. https://doi.org/10.1021/acsnano.3c03505

[43] Wong, H.S.P. and Salahuddin, S., **2015**. Memory leads the way to better computing. *Nature nanotechnology*, *10*(3), pp.191-194. https://doi.org/10.1038/nnano.2015.29

[44] Sawa, A., **2008**. Resistive switching in transition metal oxides. *Materials today*, *11*(6), pp.28-36. https://doi.org/10.1016/S1369-7021(08)70119-6

[45] Dawber, M., Rabe, K.M. and Scott, J.F., **2005**. Physics of thin-film ferroelectric oxides. *Reviews of modern physics*, *77*(4), pp.1083-1130. https://doi.org/10.1103/RevModPhys.77.1083

[46] Zubko, P., Gariglio, S., Gabay, M., Ghosez, P. and Triscone, J.M., **2011**. Interface physics in complex oxide heterostructures. *Annu. Rev. Condens. Matter Phys.*, *2*(1), pp.141-165. https://doi.org/10.1146/annurev-conmatphys-062910-140445

 © Ariston Publications 2026. All rights reserved.